



Substrate selectivity of Dengue and Zika virus NS5 polymerase towards 2'-modified nucleotide analogues



Supanee Potisophon^{a, b, 1}, François Ferron^{a, b}, Véronique Fattorini^{a, b}, Barbara Selisko^{a, b, **}, Bruno Canard^{a, b, *}

^a Aix-Marseille Université, AFMB (Laboratoire d'Architecture et Fonction de Macromolécules Biologiques) UMR 7257, 163 Avenue de Luminy, 13288 Marseille, France

^b CNRS, AFMB UMR 7257, 163 Avenue de Luminy, 13288 Marseille, France

ARTICLE INFO

Article history:

Received 5 December 2016

Received in revised form

28 December 2016

Accepted 29 December 2016

Available online 30 December 2016

Keywords:

Dengue virus

Zika virus

NS5

RNA-dependent RNA polymerase

Elongation complex

2'-modified NTP analogue

ABSTRACT

In targeting the essential viral RNA-dependent RNA-polymerase (RdRp), nucleotide analogues play a major role in antiviral therapies. In the *Flaviviridae* family, the hepatitis C virus (HCV) can be eradicated from chronically infected patients using a combination of drugs which generally include the 2'-modified uridine analogue Sofosbuvir, delivered as nucleotide prodrug. Dengue and Zika viruses are emerging flaviviruses whose RdRp is closely related to that of HCV, yet no nucleoside drug has been clinically approved for these acute infections. We have purified dengue and Zika virus full-length NS5, the viral RdRps, and used them to assemble a stable binary complex made of NS5 and virus-specific RNA primer/templates. The complex was used to assess the selectivity of NS5 towards nucleotide analogues bearing modifications at the 2'-position. We show that dengue and Zika virus RdRps exhibit the same discrimination pattern: 2'-O-Me > 2'-C-Me-2'-F > 2'-C-Me nucleoside analogues, unlike HCV RdRp for which the presence of the 2'-F is beneficial rendering the discrimination pattern 2'-O-Me > 2'-C-Me ≥ 2'-C-Me-2'-F. Both 2'-C-Me and 2'-C-Me-2'-F analogues act as non-obligate RNA chain terminators. The dengue and Zika NS5 nucleotide selectivity towards 2'-modified NTPs mirrors potency of the corresponding analogues in infected cell cultures.

© 2017 Elsevier B.V. All rights reserved.

1. Introduction

The *Flavivirus* genus comprises around 50 virus species (Gubler et al., 2007) amongst them important human pathogens such as dengue virus (DENV), yellow fever virus (YFV), West Nile virus (WNV), Japanese encephalitis virus (JEV), tick-borne encephalitis virus (TBEV), and more recently acknowledged as a significant pathogen, Zika virus (ZIKV). They belong to the *Flaviviridae* family that contains two other genera: *Hepacivirus* (main representative:

hepatitis C virus (HCV)) and *Pestivirus* (bovine viral diarrhoea virus (BVDV)) (Lindenbach and Rice, 2007).

DENV serotypes 1 to 4 are currently endemic in tropical and subtropical countries around the world (Gubler, 2011), causing dengue fever, which can develop into hemorrhagic fever and dengue shock syndrome. Despite its large burden to human health, no specific antiviral drug is currently available against this virus. Recently, a vaccine has been made available commercially, but without full protection against all serotypes (Guy et al., 2016).

ZIKV is a typical example of a re-emerging arbovirus. It was first identified in 1947 in Uganda, then detected in Micronesia in 2007, French Polynesia in 2014, and finally identified as a major public health issue in 2015 when imported to Latin America (Lessler et al., 2016). An infection with ZIKV during pregnancy is statistically associated with neonatal microcephaly and other brain anomalies (Cauchemez et al., 2016; Rasmussen et al., 2016). ZIKV is still continuing its geographical expansion, and today, more than 50 countries have reported autochthonous ZIKV cases. No vaccine or antiviral drug is on the market to specifically treat ZIKV infections.

* Corresponding author. Aix-Marseille Université, AFMB (Laboratoire d'Architecture et Fonction de Macromolécules Biologiques) UMR 7257, 163 Avenue de Luminy, 13288 Marseille, France.

** Corresponding author. Aix-Marseille Université, AFMB (Laboratoire d'Architecture et Fonction de Macromolécules Biologiques) UMR 7257, 163 Avenue de Luminy, 13288 Marseille, France.

E-mail addresses: barbara.selisko@afmb.univ-mrs.fr (B. Selisko), bruno.canard@afmb.univ-mrs.fr (B. Canard).

¹ Present address: Department of Microbiology and Immunobiology, Harvard Medical School, 77 Avenue Louis Pasteur, Boston, MA 02115, USA.

NS5 is the largest (104 kDa) and most highly conserved of the nonstructural proteins amongst the 4 DENV serotypes and within the *Flavivirus* genus. NS5 is essential for viral RNA replication. Within the flaviviral replication complex, NS5 is responsible for several enzymatic activities hosted in two domains: i) the N-terminal methyltransferase domain (NS5-MTase, residues 1–263 DENV-2, 30 kDa) and ii) the C-terminal RNA-dependent RNA polymerase (RdRp) domain (NS5-Pol, residues 272–900 DENV-2, 74 kDa) connected by a flexible linker (Lu and Gong, 2013; Saw et al., 2015; Zhao et al., 2015a, 2015b). The NS5-MTase domain catalyzes RNA cap methylation at the N7-position of the cap guanosine (N7-methylation) and the 2′O-position of the first transcribed adenosine (2′O-methylation), internal RNA methylations and has been proposed to harbor the guanylyltransferase activity (reviewed in (Dong et al., 2014) and (Decroly et al., 2011)). The NS5-Pol domain is responsible for RNA synthesis (Ackermann and Padmanabhan, 2001; Selisko et al., 2012, 2006). It is able to generate new RNA in absence of a primer, a process called *de novo* RNA synthesis. As for other RdRps starting RNA synthesis *de novo*, NS5-mediated RNA synthesis proceeds in three steps: *de novo* initiation, transition and elongation. It has been shown using purified enzyme *in vitro* that DENV NS5-Pol generates short primers (mainly pppAG) over the 3′-end of RNA templates ending in 5′-CU-3′, corresponding to the strictly conserved 3′-end of *Flavivirus* genomes and antigenomes (Selisko et al., 2012). Then the protein undergoes a transitional conformational change from the *de novo* initiation to the elongation state. Finally, it continues RNA synthesis under a processive elongation mode, *i.e.*, without dissociating significantly from its RNA template.

Steady-state kinetic studies using homo-polymeric and heteropolymeric RNA templates have been used to compare polymerase activities of full-length DENV NS5 vs. NS5-Pol (Latour et al., 2010; Lim et al., 2013; Potisopon et al., 2014). Depending on the serotype and the experimental system, the NS5-MTase domain, within the context of NS5, has been repeatedly observed to have a positive influence on NS5-Pol activity. More specifically, it was shown that the DENV-2 NS5-MTase domain stimulates RNA loading onto the adjacent polymerase domain and improves its steady-state catalytic constants both during specific *de novo* initiation and elongation reactions (Potisopon et al., 2014). For the isolated polymerase domain NS5-Pol of DENV-2, pre-steady or transient state characterization has been reported, yielding rate and affinity constants of single nucleotide incorporation by a stable binary complex made of NS5-Pol and an RNA primer/template, thus during elongation (Jin et al., 2011). The work of Jin et al. (2011) is the first example of a study of a *Flavivirus* polymerase using transient kinetic methods, *i.e.* studying an individual molecular event at a millisecond time-scale with a rapid-quench apparatus. RdRps from *Picornaviridae* and *Flaviviridae* are the only viral polymerases studied using these methods so far, pioneered by work on poliovirus RdRp (Arnold and Cameron, 2000).

In this study we set out to generate a stable elongation complex of full-length DENV-2 NS5 to study incorporation of single nucleotides and their analogues, which are potential RdRp inhibitors. During the course of our study on DENV NS5, the genome sequence of the epidemic strain of ZIKV became available (Baronti et al., 2014), allowing potentially rapid advances on ZIKV NS5 due to DENV and ZIKV relatedness in this most conserved flavivirus gene. Likewise, nucleoside analogues of interest against *Flaviviridae* are currently tested against ZIKV infected cells (Eyer et al., 2016; Zmurko et al., 2016), raising interest to understand the molecular basis of nucleoside analogue susceptibility across the *Flavivirus* genus. ZIKV NS5 has not been purified nor characterized so far, whereas recombinant DENV NS5 was first expressed and purified two decades ago (Tan et al., 1996), and is the subject of a growing

body of work. DENV and ZIKV NS5 are closely related as illustrated in Supplementary Fig. S1 by a structure-based sequence alignment and phylogenetic tree of NS5-Pol of selected flaviviruses and NS5B of HCV. Likewise, sequence alignment of full-length NS5 identifies DENV4 and WNV as the closest neighbors of ZIKV with 68% and 70% identity, respectively (See Supplementary Fig. S1A). Any DENV NS5 structural and functional data thus bear potential to be valid for ZIKV NS5. Previous studies have shown that the nucleotide analogues 2′-O-Me-CTP, 2′-C-Me-CTP, and 2′-C-Me-2′-F-CTP are substrates for incorporation into nascent RNA by the HCV RdRp NS5B (Dutartre et al., 2006; Fung et al., 2014). Likewise, 2′-C-Me-2′-F-UTP, the active 5′-triphosphate metabolite of the clinically-approved nucleotide prodrug Sofosbuvir, is a potent RNA chain-terminator substrate of the HCV polymerase NS5B (Fung et al., 2014). Sofosbuvir is clinically relevant in the fight against HCV (Coats et al., 2014). Additionally, 2′-C-Me-CTP has been reported to be active against DENV and other flaviviruses in infected cells (Deval et al., 2014). Given the structural and functional relatedness of HCV, DENV, and ZIKV RdRps, it is of interest to compare the substrate efficiency of these analogues relative to each other and to their natural counterpart. Another interesting question is if the 2′ analogues act as non-obligate RNA chain terminators in *Flavivirus* RdRps. A non-obligate chain terminator means that the incorporated nucleotide acts as a chain terminator even though the 3′-OH is available for chain elongation. Evaluating differences, if any, between HCV, DENV, and ZIKV RdRp nucleotide selectivity will help the design of a pan-flavivirus drug as well as provide a molecular basis for drug re-purposing.

Here, we prepare and characterize an active elongation complex made of full-length either DENV NS5 or ZIKV NS5 with an respective specific RNA primer/template. After assembly, the NS5-RNA complex allows the measurement of NTP incorporation. This experimental setting allowed us to study the selectivity of the DENV and ZIKV NS5 active site for several nucleotide analogues bearing a chemical modification at their 2′-position, including 2′-C-Me-2′-F-UTP (named Sofosbuvir triphosphate throughout).

2. Materials and methods

2.1. Nucleic acids

RNA oligonucleotides of 18–27 nucleotides (nt) corresponding to the 3′-end of the DENV-2 antigenome were used as templates (T₁₈ to T₂₇) annealed to 8-14-mer primers (P₈ to P₁₄) corresponding to the 5′-end of the genome. Possible secondary structures with negative free energies at 1 M NaCl were proposed by Mfold (Zuker, 2003) only for T₂₀ (stem loop at the 5′-end of ΔG -1.4 kcal/mol) and T₂₇ (5′ end ΔG -1.1 kcal/mol). Sequences of an RNA oligonucleotide template of 20 nt correspond to the 3′-end of the ZIKV antigenome (T_{Z20}); and 10- and 11-mer primers (P_{Z10}, P_{Z11}) correspond to the 5′-end of the ZIKV genome. No secondary structure with negative free energy was calculated by Mfold for T_{Z20}. RNA oligonucleotides were purchased from Biomers.net.

The 5′-end labelling reactions of the primers were done with T4 polynucleotide kinase (New England Biolabs) and [γ -³²P]-ATP (PerkinElmer) according to the manufacturer. To prepare the double-stranded RNA substrate, 5′-end radiolabeled primers were mixed with templates at a molar ratio of 1:1.5, respectively, in the presence of 110 mM KCl, incubated at 70 °C for 10 min, cooled down slowly to room temperature and then left overnight at 4 °C. The melting temperatures under annealing conditions (32 μ M P/T in 110 KCl solution) were calculated to be: P₈ 32 °C, P₁₀ 47 °C, P₁₁ 52 °C, P₁₂ 56 °C, P₁₄ 61 °C (nearest neighbor method (Kibbe, 2007)).

NTPs and 2′-O-Me-CTP were purchased from GE Healthcare and Jena Bioscience, respectively. 2′-C-Me-CTP and 2′-C-Me-2′-F-CTP

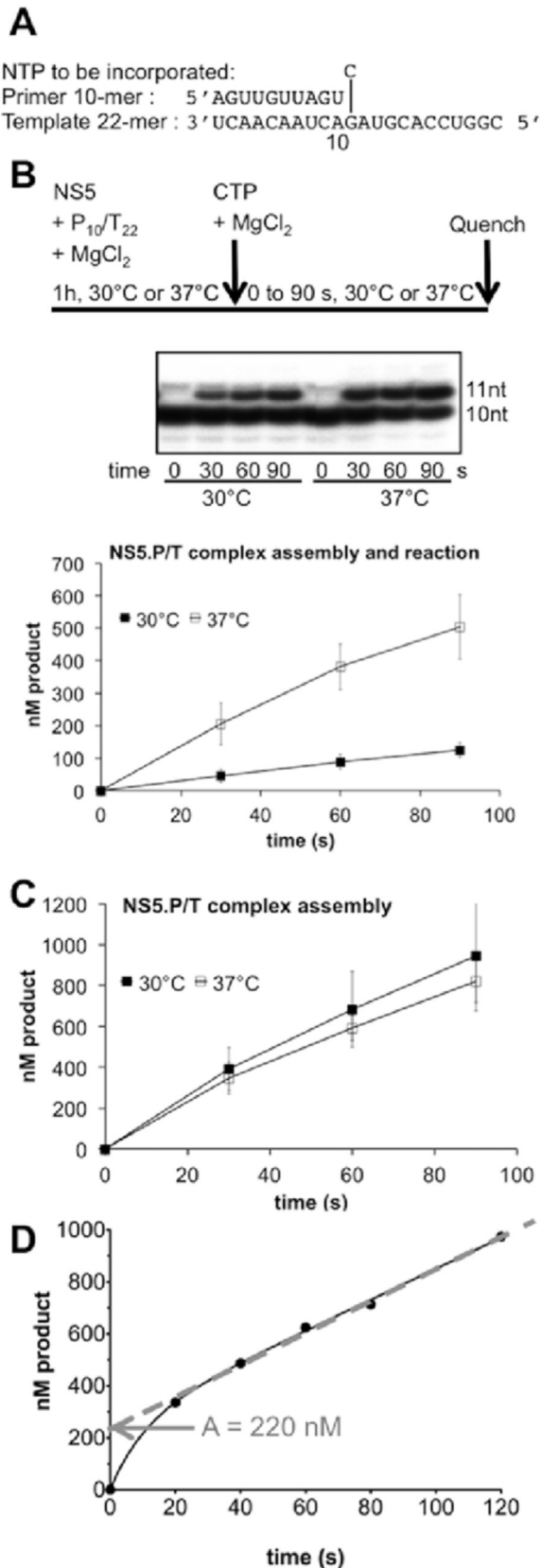


Fig. 1. Optimization of temperature and buffer conditions of DENV NS5 elongation complex assembly and reaction. Reactions were done as detailed in Methods. **A**) P₁₀/T₂₂ is a specific DENV RNA primer/template combination corresponding to the 5'-end of DENV-2 genome annealed to the 3'-end of the antigenome. CTP is added to the complex to incorporate CMP at position 11 of the primer. **B**) A schematic

and -UTP were produced, purified and HPLC-controlled at Alios BioPharma.

2.2. Protein expression and purification

The gene coding for N-terminal His₆-tagged DENV NS5 (serotype 2, strain New Guinea C) was cloned in a pQE30 expression plasmid (Selisko et al., 2006). Protein was produced in *E. coli* NEB Express (New England Biolabs) cells transformed with the pRar-e2LacI (Novagen). Cells were grown in Luria broth until the OD₆₀₀ value reached 0.6. Protein expression was then induced by 50 μM IPTG after addition of EtOH to a final concentration of 2%. Expression cultures were incubated at 4 °C during 2 h, and then shaken overnight at 17 °C. After centrifugation the cell pellets (stored at –80 °C) from 2 l bacterial culture were resuspended in 40 ml lysis buffer (50 mM sodium phosphate pH 7.5, 500 mM NaCl, 20% glycerol, 0.8% Igepal, 10 μg/ml DNase I, 0.2 mM benzamidine, 5 mM β-mercapthoethanol and 1 mg/ml lysozyme). After 40 min of incubation at 4 °C, the cell lysate was sonicated and cleared by centrifugation. The supernatant was incubated in batch with 3 ml TALON metal-affinity resin slurry (Clontech) during 1.5 h at 4 °C. Beads were washed once with washing buffer (50 mM sodium phosphate pH 7.5, 20% glycerol, 0.8% Igepal, 5 mM β-mercapthoethanol, 1 M NaCl and 10 mM imidazole) and once with washing buffer without Igepal. The protein was eluted with washing buffer containing 500 mM NaCl, 250 mM imidazole and 250 mM glycine. Size exclusion chromatography (SEC) was used as a second purification step using a Superdex 200 HR 16/20 column (GE Healthcare) and SEC buffer (50 mM HEPES pH 7.5, 300 mM NaCl, 10% glycerol, 1 mM DTT).

The synthetic ZIKV NS5 gene cloned in a pQE30 expression plasmid was obtained from Genescript. The sequence used was from strain H/PF/2013 from French Polynesia, Genbank acc# KJ776791. The ZIKV NS5, carrying His₆-tag at its N-terminus, was produced as described above for DENV NS5 with the exception that IMAC TALON beads were washed with 1.5 M NaCl. SEC was performed using a Superdex S75 HR 16/20 column (GE Healthcare) with SEC buffer 50 mM HEPES pH 7.5, 750 mM NaCl, 10% glycerol, 10 mM DTT.

After the second purification step proteins were concentrated up to around 8 mg/ml (78 μM NS5) and stored at –20 °C after adding glycerol to a final concentration of 40%. Protein purity was higher than 95% as judged by SDS-PAGE. Protein stock concentrations were determined by absorbance measurements at 280 nm using a Nanodrop 2000 (Thermo Scientific).

2.3. Optimization of NS5 elongation complex assembly and reaction

DENV NS5 elongation complexes using P₁₀/T₂₂ were first preformed in E.P/T buffer (50 mM HEPES, pH 8.0, 10% glycerol, 5 mM DTT, 5 mM MgCl₂) for different time intervals at 30 or 37 °C. Reactions were then started by adding NTP using an equal volume of NTP buffer of the same composition as the E.P/T buffer except for a higher concentration (15%) of glycerol making up for the glycerol

representation of the NS5 elongation complex assay is given in the upper panel. The middle panel shows a time course of production formation when both assembly and reaction are conducted at the same temperature, 30 °C or 37 °C, and subsequently analyzed using PAGE. Radiolabeled primer (10 nt) and the single-nucleotide elongation product (11 nt) are shown. The graph in the lower panel shows the concentration of elongation product, as quantified from gel, plotted against reaction time. **C**) Comparison of elongation product formation when the assembly step is done at 30 °C or 37 °C. Reaction is done in both cases at 37 °C. **D**) Burst-like kinetics of elongation product formation with time (optimized buffer conditions given in Methods) generated by 220 nM functional elongation complex.

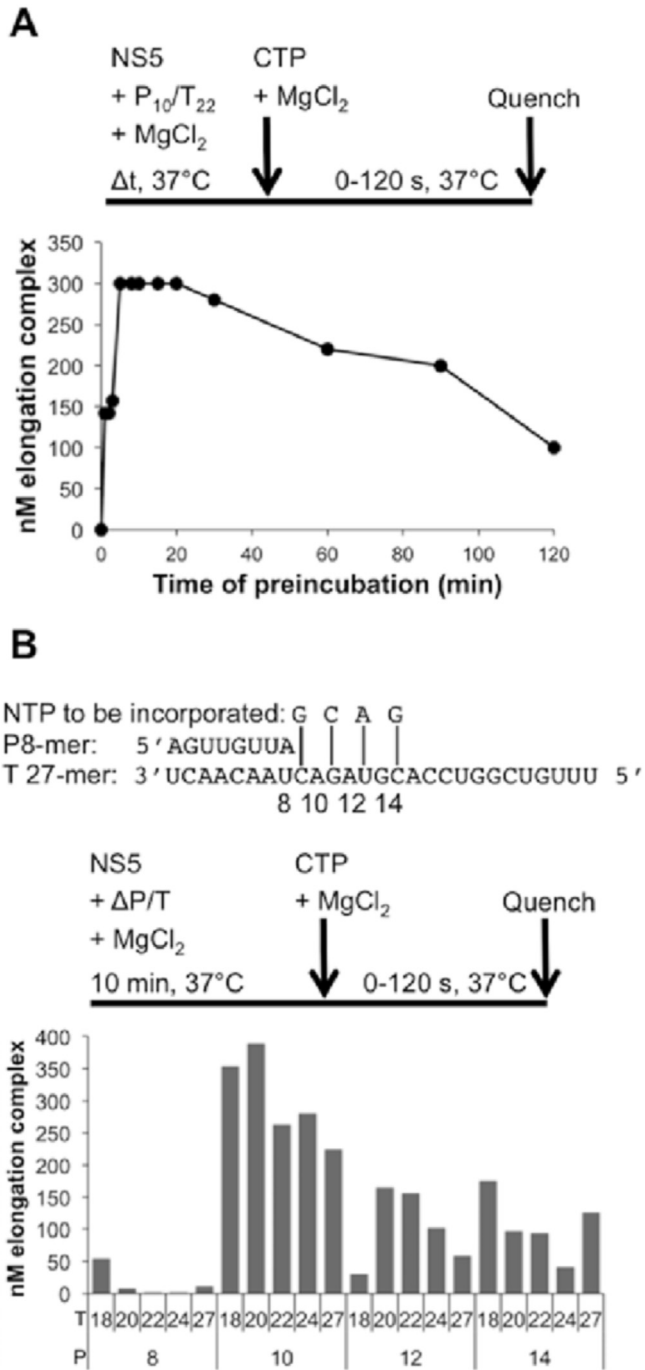


Fig. 2. Optimization of DENV NS5 elongation complex assembly time and primer/template combination. A) Optimization of pre-incubation time. Reaction conditions are given in Methods. The upper panel illustrates the reaction scheme. In the lower panel the concentration of functional elongation complex is plotted against pre-incubation time. B) Primer/template optimization. Reaction conditions are given in Methods. The upper panel gives the tested P/T combinations and the corresponding NTPs to be incorporated. The middle panel shows the reaction scheme of the NS5 elongation complex assay. The graph in the lower panel gives the concentration of functional elongation complex obtained with each combination.

present in the NS5 samples. For temperature and assembly time optimization, final concentrations in the reaction were 2 μM DENV NS5, 1.2 μM (Fig. 1B) or 3 μM P₁₀/T₂₂ (Fig. 1C) and 400 μM CTP. Final salt concentrations were 15 mM NaCl and 2.5 mM KCl coming from protein storage buffer and annealing mixture, respectively. For

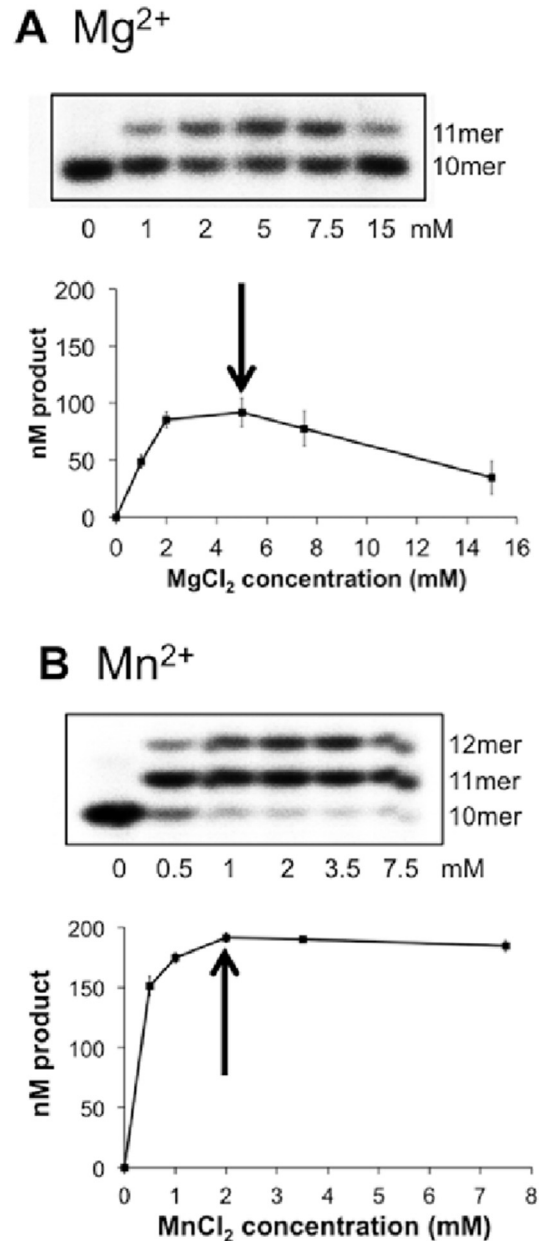


Fig. 3. Optimal assembly and elongation activity of the DENV-2 NS5-P₁₀/T₂₀ complex at 5 mM MgCl₂ and 2 mM MnCl₂. The reactions were done as detailed in Methods at given MgCl₂ or MnCl₂ concentrations. A) PAGE analysis of primer conversion after 60 s in the presence of 0–15 mM MgCl₂ (upper panel). Graphic representation of the MgCl₂ optimum (lower panel) based on the quantification of product bands after 60s reaction time. Standard deviations represent two or three independent tests. B) PAGE analysis of primer conversion after 60 s in the presence of 0–7.5 mM MnCl₂ (upper panel). Graphic representation of the MnCl₂ optimum (lower panel) based on the quantification of product bands after 60s reaction time. Standard deviations represent two or three independent tests.

buffer optimization, different concentrations were tested of DTT (0, 3, 5, 10 mM) and glycerol (5, 10, 15, 20, 25%) during both assembly and reaction. HEPES buffer was tested at pH values of 7.0, 7.5 and 8.0 and Tris buffer at pH 7.5. Samples (8 μl) were taken at given time points, added to 16 μl formamide/EDTA gel loading buffer (quenching solution) and analyzed by PAGE using polyacrylamide sequencing gels of 20% acrylamide:bisacrylamide (19:1), 8 M urea with TTE buffer (89 mM Tris pH 8.0, 28 mM taurine (2-aminoethanesulfonic acid), 0.5 mM EDTA). RNA product bands

were visualized using photo-stimulated plates and the Fluorescent Image Analyzer FLA3000 (Fuji) and quantified using Image Gauge (Fuji). The optimized conditions correspond to 37 °C during assembly and reaction, 10 min pre-incubation and an assembly and reaction buffer of 50 mM HEPES, pH 7.5, 15% glycerol, 5 mM DTT, 5 mM MgCl₂. DENV primer/template combinations of different lengths (Fig. 2B) were tested in this buffer using final concentrations in the reaction mixture of 2 μM NS5, 500 nM P/T and 400 μM CTP.

Ion dependency of assembly and/or elongation reaction were tested using 1 μM DENV NS5, 200 nM P₁₀/T₂₀ and 200 μM CTP (Figs. 3 and 4). For ZIKV NS5 the optimum conditions of DENV NS5 were used regarding buffer, temperature, and time of pre-incubation. The ion dependency of combined assembly and elongation reaction was determined using 1 μM ZIKV NS5, 200 nM P_{Z10}/T_{Z20} and 200 μM CTP (Fig. 5).

2.4. Pre-steady state analysis of nucleotide incorporation

When a productive polymerase/nucleic acid binary complex is assembled and the following nucleotide incorporation step is much faster than dissociation of the binary complex, product formation is biphasic with time, with a rapid burst phase followed by a slower, linear phase. The overall product formation can be fitted to a burst equation ($P = A(1 - \exp(-k_{obs}t) + k_{ss}t)$), where (A) is the amplitude of the product formation during the burst phase, k_{obs} is the observed rate constant of product formation during the burst phase and k_{ss} is the observed steady-state rate constant of product formation during the second, linear steady-state phase. The amplitude (A) of the burst phase corresponds to the concentration of the functional pre-assembled elongation complex, *i.e.*, the active ternary complex. We did not measure kinetic parameters during the burst phase. However, the amplitude (A) of the burst phase was estimated visually on product-over-time plots by extrapolation of the linear phase back to the Y-intercept, and taken as diagnostics that a productive ternary complex was indeed formed (Fig. 1D).

2.5. Nucleotide analogue incorporation and chain termination assays

Incorporation of CTP, 2'-O-Me-CTP, 2'-C-Me-CTP, or 2'-C-Me-2'-F-CTP into DENV P₁₀/T₂₀ and ZIKV P_{Z10}/T_{Z20} by DENV NS5 and ZIKV NS5, respectively, were measured after complex assembly under optimized conditions. Final concentrations during elongation reactions were 1 μM DENV or ZIKV NS5, 200 nM P/T and 200 μM NTP or analogues in 20 mM HEPES buffer pH 7.5 containing 15% glycerol, 5 mM DTT and the given concentrations of catalytic ions. The incorporation of UTP after CTP or its analogues was tested by the addition of 200 μM UTP to these reactions. Incorporation of UTP and analogue 2'-C-Me-2'-F-UTP was tested under the same conditions using P₁₁/T₂₀ and P_{Z11}/T_{Z20} with DENV NS5 and ZIKV NS5, respectively. The incorporation of ATP (DENV) or GTP (ZIKV) after UTP or its analogue was tested by the addition of 200 μM ATP or GTP to the reactions.

2.6. Structural modeling of the ZIKV NS5 polymerase domain

The ZIKV NS5 sequence was taken from UNIPROT (Q32ZE1: residues 2517–3419). We analyzed the sequence using the method described in Ferron et al. (2005) to define a polymerase domain of 639 amino acids including the linker (2781–3419). The sequence corresponding to this domain was submitted to the phyre2 server (Kelley et al., 2015), which generated a model from 5 templates from JEV, WNV and DENV (pdb: 4K6M/2J7U/2HFZ/5CCV/4V0Q) to maximize confidence, percentage identity and alignment coverage. The generated model had 99% of the residues modeled at more than 90% confidence. Visual inspection led us to reshape loops (residues 2757–2765 and 3047–3060) in the tunnel where the RNA template is channeled into the active site. To do so, we used Modeller V9.17 (Sali and Blundell, 1993) and energy minimized the final model using AMBER (Lindorff-Larsen et al., 2010). The final model with RNA and Sofosbuvir diphosphate (2'-C-Me-2'-F-UDP) was obtained by superimposing the HCV NS5B polymerase structure in complex

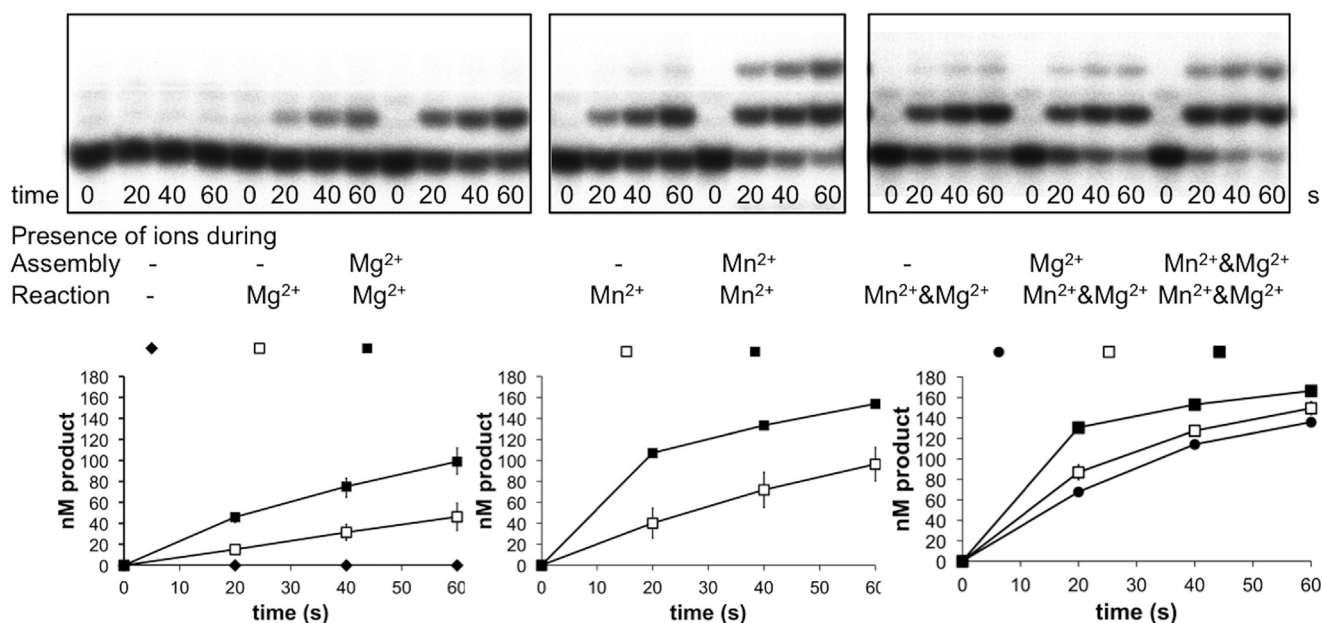


Fig. 4. Requirement of divalent ions during DENV NS5-P/T complex assembly and/or elongation reaction. Assembly and reactions were done as detailed in Methods. Briefly, the final reaction mixtures contained 1 μM NS5, 200 nM P₁₀/T₂₀, 200 μM CTP in 20 mM HEPES buffer pH 7.5, 15% glycerol, 5 mM DTT, 5 mM MgCl₂ and/or 2 mM MnCl₂ added during assembly and/or reaction as indicated. **A)** PAGE analysis of primer conversion after 0, 20, 40, 60 s in the presence of Mg²⁺ (left), Mn²⁺ (middle) as well as Mg²⁺ and Mn²⁺ (right). **B)** The molar concentration of elongation products for each condition was determined and plotted against time. Standard deviations represent two independent tests.

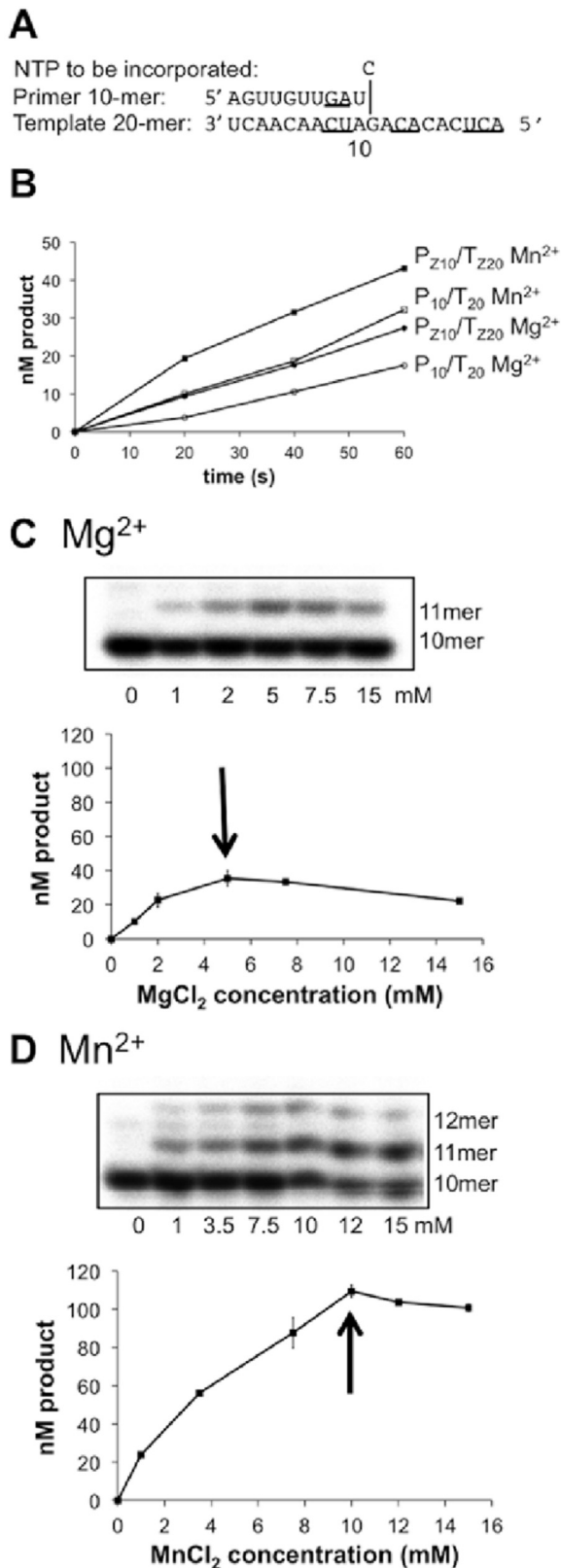


Fig. 5. Optimal pre-steady state activity of the ZIKV NS5- P_{Z10}/T_{Z20} complex at 5 mM $MgCl_2$ and 10 mM $MnCl_2$. The reactions were done as detailed in Methods at given $MgCl_2$ or $MnCl_2$ concentrations. **A)** P_{Z10}/T_{Z20} is a specific ZIKV RNA primer/template combination corresponding to the 5'-end of ZIKV genome annealed to the 3'-end of the antigenome. CMP is incorporated at position 11. Differences to the DENV P_{10}/T_{20} are underlined (compare to Fig. 1A). **B)** CMP incorporation kinetics by ZIKV NS5 using the specific ZIKV P_{Z10}/T_{Z20} or the DENV P_{10}/T_{20} . Reactions were done at 5 mM $MgCl_2$ or

with RNA and Sofosbuvir diphosphate (pdb: 4WTG) to the ZIKV polymerase model. RNA and compound were merged into the model, consistency of charges and distances between the substrate and protein were checked and the final model was energy minimized. All visual inspections, analysis, superposition and Fig. 9 were done using Chimera (Pettersen et al., 2004).

3. Results

3.1. Assembly of a functional elongation complex made of DENV NS5 and substrate RNA

In order to assemble a functional elongation complex of DENV NS5, we made use of a 5'-end radiolabeled 10-nt primer corresponding to the 5'-end of the DENV-2 genome annealed to a complementary 22-nt template corresponding to the 3'-end of the antigenome (Fig. 1A). The primer/template (P_{10}/T_{22}) was pre-incubated with NS5 in the presence of 5 mM $MgCl_2$ (see Methods). We first tested the overall effect of temperature (30 °C or 37 °C) on both assembly and reaction of the NS5 elongation complex. After complex assembly at either 30 °C or 37 °C during 1 h, the reaction was started by the addition of CTP at the same temperature. Samples were quenched at various time points and analyzed using PAGE. A temperature of 37 °C provides 4- to 5-fold more product than 30 °C (Fig. 1B). To determine which step was temperature-stimulated, we assembled the complex at 30 °C or 37 °C and challenged it with CTP at 37 °C (Fig. 1C). No significant difference in product abundance is noted, indicating that reaction rate, not complex assembly, is stimulated by temperature. We then optimized assembly and reaction using different buffer conditions as detailed in Methods. The optimized final conditions for efficient elongation are 50 mM HEPES, pH 8.0, 15% glycerol, 5 mM DTT and 5 mM $MgCl_2$.

As a next step using these optimized conditions we verified that the elongation complex allowed fast incorporation of CTP relative to its equilibrium of assembly-disassembly. A burst of product formation occurs when dissociation of the pre-formed enzyme/RNA substrate (elongation complex) is much slower than creation of the phosphodiester bond yielding an NMP-extended primer. Burst kinetics thus comprises an initial high-velocity step of addition of the NMP to the primer in the elongation complex, followed by a linear steady-state phase corresponding to dissociation of the enzyme from the extended primer/template, re-assembly of new complexes and subsequent incorporation. Kinetics of product formation was followed between 20 and 120 s (Fig. 1D). The intercept of the steady-state linear slope (see Methods) shows an approximate amplitude value of the burst phase of 220 nM. This corresponds to the concentration of active ternary elongation complex. Thus ~11% of the 2 μ M of NS5 are productively engaged under the applied reaction conditions (1.2 μ M P/T) into such a complex.

Elongation complex assembly was then further optimized, and its stability was tested comparing the resulting concentration of functional complex after different pre-incubation times (Fig. 2A). Maximum efficiency of the assembled elongation complex is reached after 10 min. The complex is stable at least 30 min at 37 °C, long enough to perform pre-steady state reactions. We also

2 mM $MnCl_2$. **C)** PAGE analysis of primer conversion after 60 s in the presence of 0–15 mM $MgCl_2$ (upper panel). Graphic representation of the $MgCl_2$ optimum (lower panel) based on the quantification of product bands after 60s reaction time. Standard deviations represent two or three independent tests. **D)** PAGE analysis of primer conversion after 60 s in the presence of 0–15 mM $MnCl_2$ (upper panel). Graphic representation of the $MnCl_2$ optimum (lower panel) based on the quantification of product bands after 60 s reaction time. Standard deviations represent two or three independent tests.

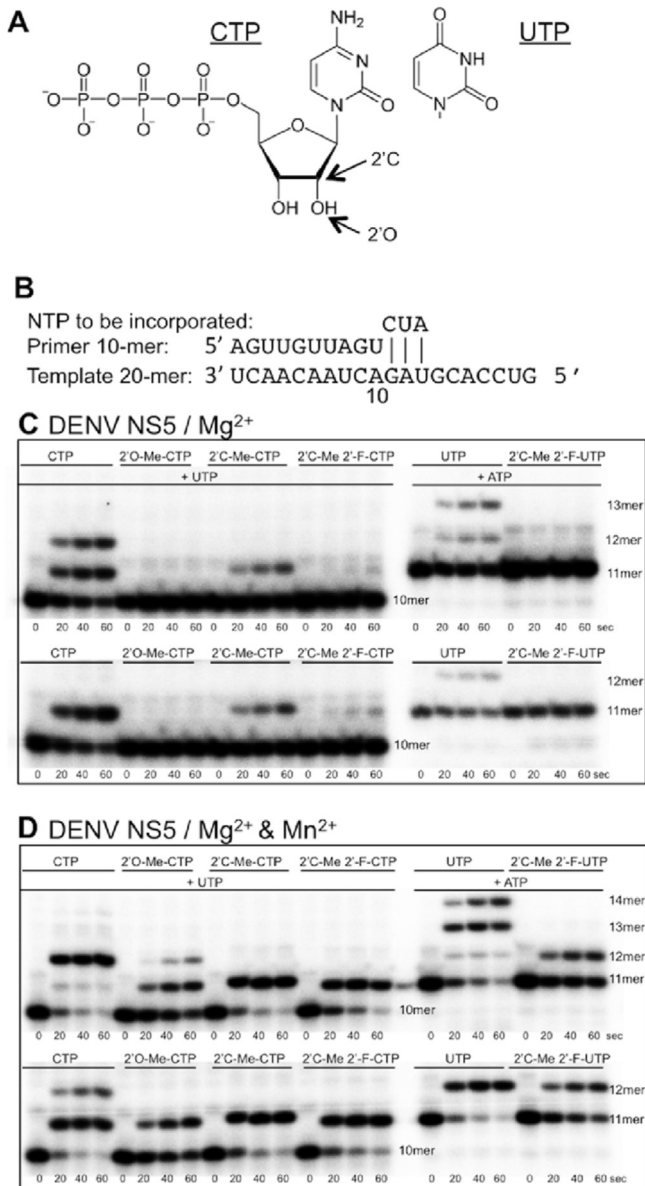


Fig. 6. Incorporation of CTP, 2'-O-Me-CTP, 2'-C-Me-CTP and 2'-C-Me-2'-F-CTP into P₁₀/T₂₀ as well as UTP and 2'-C-Me-2'-F-UTP into P₁₁/T₂₀ by DENV NS5 under elongation mode. **A**) Schematic structure representation of CTP and UTP and tested analogues **B**) Schematic representation of P₁₀/T₂₀ illustrating single incorporation assays using CTP or analogs, chain termination assays using CTP (or analogues) and UTP, single incorporation of UTP or analog into P₁₁/T₂₀ as well as chain termination assays using UTP (or analogue) and ATP. **C and D**) PAGE analysis showing the time course of CTP, 2'-O-Me-CTP, 2'-C-Me-CTP and 2'-C-Me-2'-F-CTP incorporation into P₁₀/T₂₀ in absence (lower part of the gels) and in presence (upper part of the gels) of the subsequent nucleotide UTP on left side of the gels. The right side of the gels shows the time course of UTP and 2'-C-Me-2'-F-UTP incorporation into P₁₁/T₂₀ in absence (below) and in presence (above) of the subsequent nucleotide ATP. Reactions were done as detailed in Methods. The final reaction mixtures contained 1 μM DENV NS5, 200 nM P₁₀/T₂₀ or P₁₁/T₂₀, 200 μM NTP or NTP analogues in 20 mM HEPES buffer, pH 7.5 with 30 mM glutamate/arginine, 15% glycerol, 5 mM DTT. Reactions were done in presence of 5 mM MgCl₂ (panel C) or 5 mM MgCl₂ and 2 mM MnCl₂ (panel D).

observed that after 10 min of elongation complex pre-incubation, the complex was stable at least for 1 h at 25 °C and 4 °C (data not shown).

The concentration of functional elongation complex obtained after a 10-min pre-incubation was then compared for an array of primer/template combinations (8-, 10-, 12-, 14-nt primers annealed

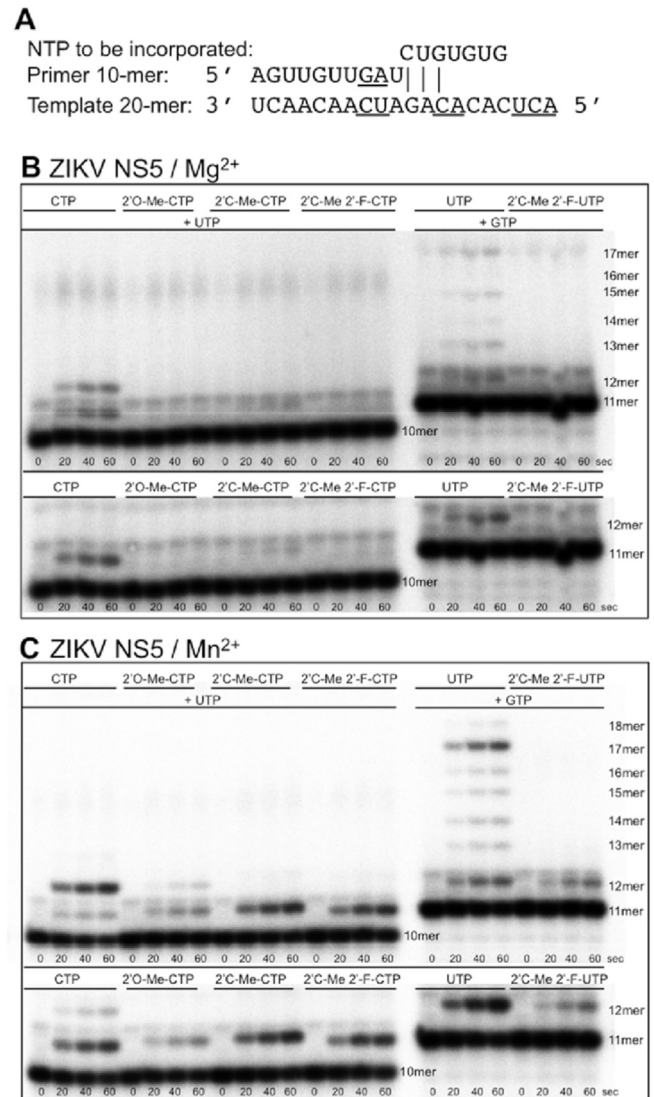


Fig. 7. Incorporation of CTP, 2'-O-Me-CTP, 2'-C-Me-CTP and 2'-C-Me-2'-F-CTP into P₂₁₀/T₂₂₀ as well as UTP and 2'-C-Me-2'-F-UTP into P₂₁₁/T₂₂₀ by ZIKV NS5 under elongation mode. **A**) Schematic representation of P₂₁₀/T₂₂₀ illustrating single incorporation assays using CTP or analogs, chain termination assays using CTP (or analogues) and UTP, single incorporation of UTP or analog into P₂₁₁/T₂₁₀ as well as chain termination assays using UTP (or analogue) and GTP. Note that multiple incorporations of U and G are possible. Sequence differences to the DENV P₁₀/T₂₀ are underlined. **B and C**) PAGE analysis showing the time course of CTP, 2'-O-Me-CTP, 2'-C-Me-CTP and 2'-C-Me-2'-F-CTP incorporation into P₂₁₀/T₂₂₀ in absence (lower part of the gels) and in presence (upper part of the gels) of the subsequent nucleotide UTP on left part of the gels. The right side of the gels shows the time course of UTP and 2'-C-Me-2'-F-UTP incorporation into P₂₁₁/T₂₂₀ in absence (below) and in presence (above) of the subsequent nucleotide GTP. Reactions were done as detailed in Methods. The final reaction mixtures contained 1 μM ZIKV NS5, 200 nM P₂₁₀/T₂₂₀ or P₂₁₁/T₂₂₀, 200 μM NTP or NTP analogues in 20 mM HEPES buffer, pH 7.5, 15% glycerol, 5 mM DTT. Reactions were done in presence of 5 mM MgCl₂ (panel B), and 10 mM MnCl₂ (panel C).

to 18-, 20-, 22-, 24- and 27-nt templates) in order to find the optimal primer/template combination (Fig. 2B). Short reaction time courses were followed after a 10-min pre-incubation period (see reaction scheme in Fig. 2B). Strikingly, a minimal primer length of 10 nucleotides is required to obtain a significant amount of reaction product. P₁₀/T₂₀ is the most efficient primer/template combination giving the highest concentration of functional elongation complex, as judged by the measurement of the concentration of elongation complex (burst amplitude). We observe up to 400 nM of the latter,

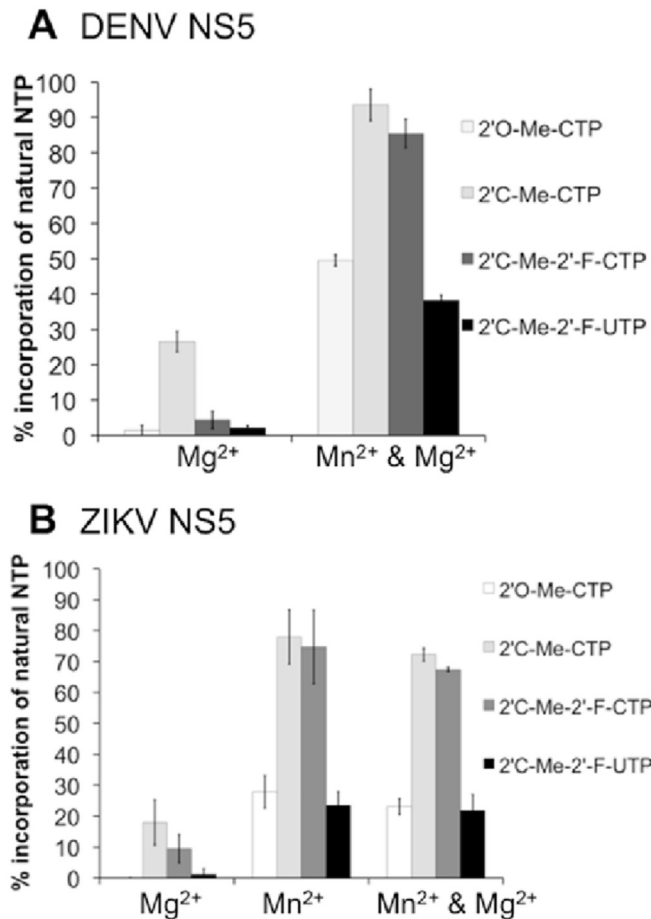


Fig. 8. Percentage of incorporation of 2'-O-Me-CTP, 2'-C-Me-CTP, 2'-C-Me-2'-F-CTP and 2'-C-Me-2'-F-UTP by DENV-2 NS5 (panel A) and ZIKV NS5 (panel B) under elongation mode in comparison to the respective natural NTPs. Data from experiments presented in Figs. 6 and 7. The presence of catalytic ions during the reactions is given in the legend. Given values are mean values of two to four independent tests in absence or presence of the following nucleotide. All product bands were taken into account. For each test the average percentage at all time points was calculated.

i.e., ~80% of the 0.5 μ M P₁₀/T₂₀ is used by 20% of a total 2 μ M NS5 present in the reaction mixture.

3.2. Metal ion dependence of DENV and ZIKV NS5 elongation complexes

It is currently not clear if for DENV and ZIKV RdRps metal ions - and which - are required for optimal complex formation or only for the elongation reaction, or both. It was reported that DENV NS5-Pol needs Mg²⁺ to form stable active elongation complexes (Jin et al., 2011). We assayed both Mg²⁺, which had been used exclusively during the optimization process, and Mn²⁺. Although the use of Mn²⁺ *in vivo* remains an open question, this metal ion is widely used in enzymatic assays of viral RdRps. A structural and functional study of a panel of viral RdRps has evidenced a conserved structural Mn²⁺ binding site, from which the Mn²⁺ plays a critical and stimulating role in the RdRp catalytic properties affecting both initiation and elongation (Poranen et al., 2008; Wright et al., 2012).

In order to study the effect of both ions on assembly and reaction, we first verified the optimum concentrations of Mg²⁺ and Mn²⁺ for overall fast nucleotide incorporation. For DENV NS5 they were found at 5 mM and 2 mM for MgCl₂ and MnCl₂, respectively (Fig. 3A and B). They are the same as those determined before for NS5-Pol using other systems (Selisko et al., 2006). In these tests we also observed that in presence of Mn²⁺ DENV NS5 generates two product bands corresponding to P₁₁ and P₁₂, the latter with a mismatched C opposite A, presumably. The higher possibility of mismatch incorporation in the presence of Mn²⁺ by viral RdRps has been reported before (Arnold et al., 1999; Huang et al., 1997; Shim et al., 2002). Both product bands were considered for the quantification of primer conversion and the concentration of productive elongation complex. We then tried to dissociate assembly from reaction (Fig. 4) using the determined optimum concentrations of either Mg²⁺ or Mn²⁺ or both. Indeed, since the elongation reaction time is at least 10 times shorter than that of assembly, any further complex assembly occurring during elongation is negligible. As expected we see that the presence of either Mg²⁺ or Mn²⁺ is essential for the elongation reaction (absence of product when no ion is used during elongation but product accumulation when ions

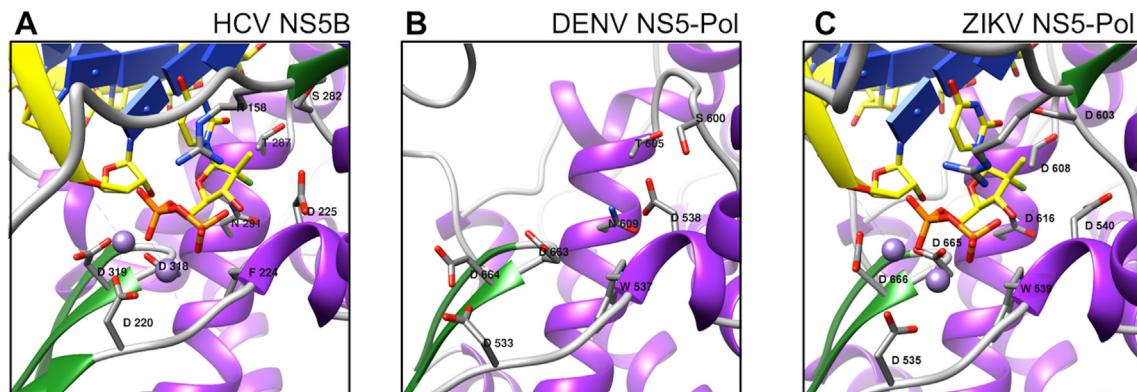


Fig. 9. Comparison of Flaviviridae polymerase active site pockets. **A)** Zoom onto the HCV NS5B RdRp active site in complex with a primer/template RNA and 2'-C-Me-2'-F-UDP, Sofosbuvir diphosphate (4WTG). Active site residues D318, D319 (catalytic motif C), D220, F224, D225 (motif A), S282, T287, N291 (motif B) and R158 (motif F) are shown. **B)** Zoom of DENV NS5 polymerase active site (4VOQ) in the same orientation as HCV NS5B in panel A. Note that motif F is not in place in all DENV NS5 structures to date. **C)** Zoom on the active site of a complex of the ZIKV NS5 RdRp domain model with superimposed RNA and Sofosbuvir diphosphate from 4WTG in the same orientation as HCV NS5B in panel A. Note that motif F is in place adapted from the JEV NS5 structure during the modeling by phyre2 (see Methods). For the three panels, secondary structures are colored as follows: β -strands in green, α -helices in purple, loops in grey. The phosphate backbone of the RNA primer/template is represented as a yellow tube; the bases are represented by blue rectangles, the riboses in sticks. Sofosbuvir diphosphate is shown in sticks with carbon atoms in yellow, phosphorus atoms in red, oxygen in red and fluorine in green. Side chains of key residues are labeled by one-letter codes and corresponding residue numbers; and atoms are colored as: carbon in grey, oxygen in red and nitrogen in blue. (For interpretation of the references to colour in this figure legend, the reader is referred to the web version of this article.)

are present during elongation). Additionally, the absence of any ion during complex assembly always generates less product than when ions are present. Ions are thus involved to promote assembly of an active complex as well as to generate a burst of product formation. Mn^{2+} activates assembly and reaction to a higher degree than Mg^{2+} (Fig. 4, compare left and middle panel), which is further shown in the right panel (compare assembly in the presence of Mg^{2+} or Mg^{2+} & Mn^{2+}). Similar to what is observed in Fig. 3, the presence of Mn^{2+} is linked to the appearance of mis-incorporation 12-mer products, as observed for other polymerases (Arnold et al., 1999; Huang et al., 1997; Shim et al., 2002). Product generation in the presence of both cations during assembly and/or reaction does not deviate from what is observed when Mn^{2+} alone is used (compare middle and right panel).

For ZIKV NS5 we used complex assembly and elongation reaction conditions optimized for DENV-2 NS5. However, as ZIKV NS5 is less active on DENV sequence templates than on its own authentic sequences, a specific ZIKV primer/template combination was used (Fig. 5A and B). The optimum ion concentrations for ZIKV NS5 during elongation complex assembly and reaction are 5 mM $MgCl_2$ and 10 mM $MnCl_2$ (Fig. 5C and D, respectively). Thus interestingly, the $MnCl_2$ optimum concentration of ZIKV NS5 for elongation complex assembly and reaction is 5-fold higher than for DENV-2 NS5 (2 mM $MnCl_2$ see Fig. 3B).

3.3. CTP and UTP analogue selectivity by DENV and ZIKV NS5

We aimed at determining the pre-steady state constants of 2'-modified nucleotide analogues in order to relate them to their antiviral properties. Although fast NTP incorporation occurred after assembly of the functional elongation complex, we noted that the complex precipitated as the solution became turbid during pre-incubation of NS5 with primer/template RNA at 37 °C. The phenomenon of a functional precipitated RdRp-RNA elongation complex has been described for both HCV NS5B (Jin et al., 2012) and full-length JEV NS5 (Wu et al., 2015). Precipitation of the binary complex precluded the use of fast mixing/quenching equipment required to determine pre-steady state constants. It did not, however, impede steady state measurements (see Methods). We thus made use of this experimental set-up to compare fast nucleotide analogue incorporation efficiencies. We ran kinetic assays manually measuring NTP or analogues' incorporation after 20, 40 and 60 s. The reactions were analyzed using denaturing PAGE (Figs. 6 and 7). First, we used 1 μ M DENV NS5 together with 200 nM P_{10}/T_{20} (specific for DENV, see Fig. 6B) and 200 μ M of either CTP, 2'-O-Me-CTP, 2'-C-Me-CTP, 2'-C-Me-2'-F-CTP (Fig. 6C and D lower left part of the gels). To test potential chain-termination by these analogues, the same reactions were done in the presence of 200 μ M of UTP, the next correct nucleotide (upper left part of the gels). We then used 1 μ M DENV NS5 together with 200 nM P_{11}/T_{20} (specific for DENV, see Fig. 6B) and 200 μ M of either UTP or 2'-C-Me-2'-F-UTP (Fig. 6C and D lower right part of the gel). To test chain-termination the same reactions were done in the presence of 200 μ M of ATP, the next correct nucleotide (upper right part of the gel). For DENV NS5, incorporation and chain termination was determined at optimum concentrations of Mg^{2+} (Fig. 6C) or both Mg^{2+} and Mn^{2+} (Fig. 6D). For ZIKV NS5, we used the same set-up as for DENV but with specific ZIKV primer/templates (see Fig. 7A). To test potential chain-termination by 2'-C-Me-2'-F-UMP, the reactions were done in the presence of 200 μ M of GTP, the next correct nucleotide for ZIKV (Fig. 7B and C, upper right part of the gel). Note that the template sequence allows multiple incorporations of U and G (Fig. 7A). Incorporation and chain termination were tested at optimum concentrations of Mg^{2+} (Fig. 7B), Mn^{2+} (Fig. 7C) or both Mg^{2+} and Mn^{2+} (the gel is not shown but its product quantification is given in

Fig. 8B). Product formation at each time point was quantified and the percentage of incorporation of "natural" NTP is given in Fig. 8A for DENV NS5 and Fig. 8B for ZIKV NS5.

In the presence of Mg^{2+} (Figs. 6C and 7B as well as 8A and B) only the 2'-C-Me-CTP analogue is significantly incorporated into RNA (26.6% of CTP incorporation for DENV NS5 and 17.9% for ZIKV NS5). The additional presence of a fluorine atom at the 2'-position of either 2'-C-Me-CTP or 2'-C-Me-UTP has a negative impact on incorporation. The presence of the next correct nucleotide has no significant effect: once incorporated, 2'-C-Me-CMP terminates RNA synthesis.

In the presence of Mn^{2+} or both Mg^{2+} and Mn^{2+} (Figs. 6D, 7C and 8A and B) improved incorporation is expectedly observed as Mn^{2+} activates complex assembly and elongation reaction (see above). The presence of Mn^{2+} has been reported to decrease the substrate specificity of viral RdRps and also of DNA polymerases (Arnold et al., 2004; Vashishtha et al., 2016). Accordingly, the 2'-O-Me-CTP analogue is incorporated by DENV-2 NS5 into RNA to 49.6% compared to CTP in the presence of Mn^{2+} & Mg^{2+} . Likewise its incorporation by ZIKV NS5 in comparison to CTP is 27.8% in the presence of Mn^{2+} and 23.1% in the presence of Mn^{2+} & Mg^{2+} . Unlike its 2'-C-Me or 2'-C-Me-2'-F-counterparts, 2'-O-Me-CTP does not act as a non-obligate chain terminator, as +2 nucleotide products are readily detected. 2'-C-Me-CMP is incorporated into RNA to an extent comparable to that of the natural nucleotide CTP (93.6% by DENV-2 NS5 (in the presence of Mn^{2+} & Mg^{2+}); 77.9% (Mn^{2+}) and 72.2% (Mn^{2+} & Mg^{2+}) by ZIKV NS5). Again, the presence of a fluorine atom in 2' decreases, but does not prevent, incorporation of 2'-C-Me-2'-F-CTP (85.5% by DENV-2 NS5 in the presence of Mn^{2+} & Mg^{2+} , 74.7% (Mn^{2+}) and 67.4% (Mn^{2+} & Mg^{2+}) by ZIKV NS5). Both analogues act also in the presence of Mn^{2+} as non-obligate chain-terminators. Sofosbuvir triphosphate is less well incorporated into RNA than the corresponding CTP analogue (38.3% by DENV-2 NS5 (in the presence of Mn^{2+} & Mg^{2+}), 23.5% (Mn^{2+}) and 21.8% (Mn^{2+} & Mg^{2+}) by ZIKV NS5) and also acts as a non-obligate chain terminator.

In conclusion, we note no significant difference in substrate selectivity between DENV and ZIKV NS5. We observe the following general substrate efficiency, i.e., the opposite of discrimination, for both *Flavivirus* RdRps CTP = UTP \geq 2'-C-Me-CTP > 2'-C-Me-2'-F-CTP > 2'-C-Me-2'-F-UTP = 2'-O-Me-CTP (Fig. 8). Only 2'-O-Me-CTP does not act as a chain terminator, whereas 2'-C-Me-CTP, 2'-C-Me-2'-F-CTP and 2'-C-Me-2'-F-UTP are non-obligate RNA chain terminators.

4. Discussion

Nucleoside analogues represent first-line treatments in a variety of viral diseases, such as those caused by, e.g., the human immunodeficiency virus, herpes virus and HCV. Infections by the latter are currently successfully treated in the clinic with several drug regimens, in which nucleoside analogues occupy a prominent place. The HCV RdRp is efficiently targeted with Sofosbuvir, a uracil nucleotide analogue delivered as a prodrug. For HCV, structure-activity relationship studies on nucleoside analogues have converged to 2'-F 2'-C-Me ribose modifications (Coats et al., 2014), and the mechanism of action of the corresponding nucleotide analogue has been determined (Fung et al., 2014). Selective incorporation of the 5'-monophosphate form of the analogue into viral RNA terminates viral RNA synthesis, accounting for the antiviral effect observed in infected cells and patients. Success obtained with antiretroviral nucleoside analogues has been inspiring for the whole antiviral research field. In turn, the HCV drug-design field is now a precious guide in programs targeting phylogenetically related viruses, such as DENV. The recent emergence of ZIKV

further extends this relatedness-guided antiviral drug development, as DENV and ZIKV are closely related (see [Supplementary Fig. S1A and B](#)). Their polymerases NS5 share ~65% identity at the amino acid level. Therefore, it was of interest to characterize any potential biochemical/enzymatic difference between DENV and ZIKV RdRps in order to capitalize the growing knowledge on DENV and speed-up anti-ZIKV drug discovery.

The unavailability of recombinant full-length, stable and active *Flavivirus* RdRp has long been limiting for detailed studies on the mechanism of action of inhibitors. Most DENV RdRp studies have been performed on the RdRp domain truncated from its RNA-cap methyltransferase (MTase) domain (amino acids 1 to ~265) ([Jin et al., 2011](#)). However, the MTase domain of *Flavivirus* NS5 has been observed to stimulate overall polymerase activity supposedly through flexible internal protein-protein interfaces ([Latour et al., 2010](#); [Lim et al., 2013](#); [Potisopon et al., 2014](#)). Some interfaces which are conserved in the *Flavivirus* genus have been structurally and functionally characterized ([Klema et al., 2016](#); [Lim et al., 2013](#); [Lu and Gong, 2013](#); [Wu et al., 2015](#); [Zhao et al., 2015a, 2015b](#)). In order to determine the mechanism of action of nucleotide analogues targeting the viral polymerase, we have expressed and purified full-length DENV and ZIKV NS5 proteins to apparent homogeneity and assessed their ability to incorporate into RNA 2'-modified nucleotides that are known to inhibit HCV as well as DENV in infected cells ([Deval et al., 2014](#)).

Nucleotide analogues are best characterized using pre-steady state kinetics from which their dissociation constant K_d and catalytic constant k_{pol} are derived. Our work describes experimental conditions allowing a stable binary complex NS5.P/T to be formed, and subsequent fast incorporation of 5'-monophosphate analogues into RNA. The difficulty to obtain such complex stems from the fact that viral polymerases synthesizing RNA *de novo* have evolved mechanisms to selectively start RNA synthesis on viral RNAs. This involves sequence specific contacts as well as viral RNA structures and factors to initiate primer synthesis on viral templates preferentially. This regulation avoids spurious RNA synthesis that could both potentially ignite innate immunity mechanisms in the host cell and decrease overall viral RNA synthesis efficiency. We succeeded to assemble functional elongation complexes of DENV and ZIKV NS5 with short virus-specific primer/templates. Interestingly ZIKV NS5 seems to be sensitive to sequence differences within the first 10 nt of the genome and/or the last 20 nt of the antigenome (see [Fig. 7B](#)) suggesting that major binding determinants or regulation elements may exist along the NS5 surface, together with specific sequence elements ([Gebhard et al., 2011](#)). In line with this hypothesis, we observe that both soluble DENV and ZIKV NS5 precipitate upon binding to the specific primer/template RNA. The precipitated complex is active, and can be partially solubilized (data not shown), indicating that structural rearrangements occur that might represent the different conformational changes of NS5 performing the RNA synthesis steps necessary to faithfully copy viral RNA. It is also striking to observe that incorporation efficiencies vary widely depending on primer/template length ([Fig. 2](#)). The pair P_{10}/T_{20} provided the most efficient combination. The variation is not due to unfavorable T_m values of short P/T combinations (see Methods). Instead, loading of P_8/T_{20} may be more difficult because of a 5'-end stem loop within T_{20} that involves the entire 5' sequence stretch that is not annealed to P_8 . When P_{10}/T_{20} is used stem loop formation involving the 5'-end of T_{20} is not possible or at least should have less impact because P_{10} interferes. Overall, with the precipitated active elongation complexes of DENV NS5. P_{10}/T_{20} and ZIKV NS5. P_{210}/T_{220} complexes we were not able to determine K_d and k_{pol} values but we could study fast steady state incorporation of NTP analogues and their putative action as chain terminators.

Assembly of the functional elongation complexes made of DENV

or ZIKV NS5 and substrate RNA is at least in part controlled by the presence of a divalent metal ion, such as Mg^{2+} or Mn^{2+} . The biological availability of each metal ion, its actual use *in vivo*, and its mechanism of action within the context of the RdRp activity have been much studied and debated (see discussion in ([Selisko et al., 2012](#)) and ([Arnold et al., 2004](#); [Arnold and Cameron, 2004](#); [Poranen et al., 2008](#); [Wright et al., 2012](#))). The greater efficiency of complex assembly in the presence of Mn^{2+} leaves open the possibility that *in vivo* this ion might be used to enhance specific steps in the viral cycle, such as complex assembly, that do not compromise RNA synthesis fidelity and thus virus viability. Such selective use of Mn^{2+} has been proposed based on the crystal structure and activity of the bacteriophage Phi6 RdRp ([Poranen et al., 2008](#)). It is apparent in our results that Mn^{2+} relaxes NS5 fidelity at the elongation step. One important difference between DENV and ZIKV NS5 is the weak affinity of ZIKV NS5 to Mn^{2+} in comparison to DENV NS5 (10 mM optimum concentration versus 2 mM $MnCl_2$). If this involves complex formation or NMP incorporation is currently not clear.

Finally, we report that 2'C analogues are incorporated by DENV and ZIKV NS5 to a very low extent in the presence of Mg^{2+} and to a higher extent in the presence of Mn^{2+} . In both cases they clearly act as non-obligate chain terminators. We state a major nucleotide analogue selectivity difference in the *Flaviviridae* family between HCV RdRp and the *Flavivirus* RdRps of DENV and ZIKV. The 2'-ribose position of nucleosides has been identified very early as a promising site of chemical modification to yield analogues with good selective incorporation properties by viral, not cellular, RdRps. In the case of HCV RdRp, 2'-C-Me nucleoside inhibitor efficiency is improved when a fluorine atom is added at this position to yield 2'-C-F 2'-C-Me analogues ([Coats et al., 2014](#); [Fung et al., 2014](#)). When present on a uracil backbone and appropriately prodrugged, this modification has yielded Sofosbuvir, one of the most successful anti-HCV drug known so far. Given the structural and functional relatedness of DENV and ZIKV RdRps to HCV NS5B, it came to a surprise when we observed that the 2'-C-F modification added to the 2'-C-Me actually reduces nucleotide incorporation efficiency using the *Flavivirus* DENV and ZIKV RdRps. With the aim to understand the minute structural variations that may account for that difference, we have compared the active site of the HCV NS5B elongation complex crystal structure containing Sofosbuvir diphosphate (2'C-Me-2'-F-UDP) ([Appleby et al., 2015](#)) and of the crystal structure of the RdRp domain of DENV full-length NS5 ([Klema et al., 2016](#)) ([Fig. 9A and B](#)). In addition, we have generated a model of ZIKV RdRp domain on the basis of five available *Flavivirus* NS5 or NS5-Pol structures (see Methods) and superimposed it onto the HCV NS5B elongation complex crystal structure to obtain a complex with primer/template and 2'-C-Me-2'-F-UDP ([Fig. 9C](#)). The crystal structure of HCV NS5B shows how the nucleotide analogue fits well into the active site with no steric hindrance in the vicinity of the 2' position of the ribose impeding binding ([Fig. 9A](#)). The D225 side chain is closest to the 2' position. Based on various structures of RdRp complexes captured during the catalytic cycle and apo-structures especially from poliovirus polymerase it has been proposed ([Gong and Peersen, 2010](#)) that for all plus-strand RNA virus RdRps motif A (containing D225 and catalytic residue D220) adopts a closed conformation only when an appropriate NTP substrate is in the active site. This closed conformation allows the formation of a long β -strand that precedes motif A (see [Fig. 9A](#) in the lower left corner). Available crystal structures of the unliganded DENV NS5 RdRp domain (in the context of NS5 ([Fig. 9B](#)) and also as single domain ([Zhao et al., 2015a](#))) show a very similar pocket lined with equivalent residues but with Motif A in an open conformation. Motif A is only preceded by a short β -strand (see [Supplementary Fig. S1A](#)) and the catalytic D538 is further away. The residue spatially equivalent to HCV NS5B D225 (here D538 for DENV NS5) is

clearly facing the solvent, compared to HCV NS5B where it has to turn away from the NTP binding pocket to be able to accommodate 2'-C-Me-2'-F-UDP (Fig. 9A and B). When either the DENV structure or the ZIKV structural model in the open conformation were superimposed to the HCV NS5B-Sofosbuvir diphosphate complex, a steric clash with D540 (equivalent to DENV D538) prevented accommodation of the nucleotide analogue. Resolution of the clash was achieved through changing rotamers of D540. Sofosbuvir di- or triphosphate can be accommodated into the ZIKV polymerase active site provided that D540 is turned away (Fig. 9C). Our functional data suggest that with Sofosbuvir triphosphate (2'-C-Me-2'-F-UTP) in the active site *Flavivirus* RdRps are less efficient in this proposed subtle conformational change of motif A from the open to a closed conformation with D538 side change rotation leaving enough space for the 2'-C Me- and 2'-C F- groups. The structural reason might be the sequence differences between other motif A residues of HCV NS5B (FSYDTRHFD) and *Flavivirus* NS5 (YADD-TAGWDT) which are implicated in this conformational change (see also Supplementary Fig. S1A). As a consequence the incorporation of 2'-C-Me-2'-F-UTP is less efficient and Sofosbuvir triphosphate discrimination is different between *Hepacivirus* (HCV) and *Flavivirus* (here, DENV and ZIKV) RdRps. Accordingly, in one of the recent studies it has been reported that Sofosbuvir does not inhibit ZIKV in infected cell cultures whereas 2'-C Me cytidine does (Eyer et al., 2016).

In conclusion, we have compared at the functional level the DENV and ZIKV RdRps towards their use of nucleotide analogues clinically significant for the treatment of HCV. In addition to representing the first ZIKV full-length NS5 activity report at the molecular level, our results should help the design of pan-flavivirus drugs aiming at the control of many *Flavivirus* members of this large family of emerging arboviruses, as well as understand the basis of re-purposing drugs against emerging viral diseases.

Acknowledgments

We thank Alios BioPharma, Inc., Part of the Janssen Pharmaceutical Companies, South San Francisco, CA, USA for providing most of the 2' nucleotide analogs and especially Dr Jerome Deval for his precious help and for inspiring conversations and critically reading of the manuscript. We thank Dr Bruno Coutard for his help in obtaining the synthetic gene for ZIKV NS5. This work was supported by the Fondation pour la Recherche Médicale [Programme Equipe FRM to B. C. (DEQ20081213949) and Programme Espoirs de la Recherche to S. P. (FDT20130928186)]; by Infectiopôle-Sud [PhD scholarship to S. P.]; by the European Union Seventh Framework Programme (FP7/2007–2013) through the SILVER (Small inhibitor leads against emerging RNA viruses) project [No 260644]; by the European program H2020 under the ZIKAlliance project (grant agreement No 734548) and the EVAg Research Infrastructure (grant agreement No 653316). The funders had no role in study design, data collection and analysis, decision to publish, or preparation of the manuscript.

Appendix A. Supplementary data

Supplementary data related to this article can be found at <http://dx.doi.org/10.1016/j.antiviral.2016.12.021>.

References

Ackermann, M., Padmanabhan, R., 2001. *De novo* synthesis of RNA by the dengue virus RNA-dependent RNA polymerase exhibits temperature dependence at the initiation but not elongation phase. *J. Biol. Chem.* 276, 39926–39937. <http://dx.doi.org/10.1074/jbc.M104248200>.

Appleby, T.C., Perry, J.K., Murakami, E., Barauskas, O., Feng, J., Cho, A., Fox, D.,

Wetmore, D.R., McGrath, M.E., Ray, A.S., Sofia, M.J., Swaminathan, S., Edwards, T.E., 2015. Viral replication. Structural basis for RNA replication by the hepatitis C virus polymerase. *Science* 347, 771–775. <http://dx.doi.org/10.1126/science.1259210>.

Arnold, J.J., Cameron, C.E., 2004. Poliovirus RNA-dependent RNA polymerase (3Dpol): pre-steady-state kinetic analysis of ribonucleotide incorporation in the presence of Mg²⁺. *Biochem. Mosc.* 43, 5126–5137. <http://dx.doi.org/10.1021/bi035212y>.

Arnold, J.J., Cameron, C.E., 2000. Poliovirus RNA-dependent RNA polymerase (3D(pol)). Assembly of stable, elongation-competent complexes by using a symmetrical primer-template substrate (sym/sub). *J. Biol. Chem.* 275, 5329–5336.

Arnold, J.J., Ghosh, S.K., Cameron, C.E., 1999. Poliovirus RNA-dependent RNA polymerase (3D(pol)). Divalent cation modulation of primer, template, and nucleotide selection. *J. Biol. Chem.* 274, 37060–37069.

Arnold, J.J., Gohara, D.W., Cameron, C.E., 2004. Poliovirus RNA-dependent RNA polymerase (3Dpol): pre-steady-state kinetic analysis of ribonucleotide incorporation in the presence of Mn²⁺. *Biochem. Mosc.* 43, 5138–5148. <http://dx.doi.org/10.1021/bi035213q>.

Baronti, C., Piorowski, G., Charrel, R.N., Boubis, L., Leparç-Goffart, I., de Lamballerie, X., 2014. Complete coding sequence of zika virus from a French Polynesia outbreak in 2013. *Genome Announc.* 2. <http://dx.doi.org/10.1128/genomeA.00500-14>.

Cauchemez, S., Besnard, M., Bompard, P., Dub, T., Guilletette-Artur, P., Eyrolle-Guignot, D., Salje, H., Van Kerkhove, M.D., Abadie, V., Garel, C., Fontanet, A., Mallet, H.-P., 2016. Association between Zika virus and microcephaly in French Polynesia, 2013–15: a retrospective study. *Lancet Lond. Engl.* 387, 2125–2132. [http://dx.doi.org/10.1016/S0140-6736\(16\)00651-6](http://dx.doi.org/10.1016/S0140-6736(16)00651-6).

Coats, S.J., Garnier-Amblard, E.C., Amblard, F., Ehteshami, M., Amiralaie, S., Zhang, H., Zhou, L., Boucle, S.R.L., Lu, X., Bondada, L., Shelton, J.R., Li, H., Liu, P., Li, C., Cho, J.H., Chavre, S.N., Zhou, S., Mathew, J., Schinazi, R.F., 2014. Chutes and ladders in hepatitis C nucleoside drug development. *Antivir. Res.* 102, 119–147. <http://dx.doi.org/10.1016/j.antiviral.2013.11.008>.

Decroly, E., Ferron, F., Lescar, J., Canard, B., 2011. Conventional and unconventional mechanisms for capping viral mRNA. *Nat. Rev. Microbiol.* 10, 51–65.

Deval, J., Symons, J.A., Beigelman, L., 2014. Inhibition of viral RNA polymerases by nucleoside and nucleotide analogs: therapeutic applications against positive-strand RNA viruses beyond hepatitis C virus. *Curr. Opin. Virol.* 9, 1–7. <http://dx.doi.org/10.1016/j.coviro.2014.08.004>.

Dong, H., Fink, K., Züst, R., Lim, S.P., Qin, C.-F., Shi, P.-Y., 2014. Flavivirus RNA methylation. *J. Gen. Virol.* 95, 763–778. <http://dx.doi.org/10.1099/vir.0.062208-0>.

Dutartre, H., Bussetta, C., Boretto, J., Canard, B., 2006. General catalytic deficiency of hepatitis C virus RNA polymerase with an S282T mutation and mutually exclusive resistance towards 2'-modified nucleotide analogues. *Antimicrob. Agents Chemother.* 50, 4161–4169. <http://dx.doi.org/10.1128/AAC.00433-06>.

Eyer, L., Nencka, R., Huvarová, I., Palus, M., Joao Alves, M., Gould, E.A., De Clercq, E., Růžek, D., 2016. Nucleoside inhibitors of Zika virus. *J. Infect. Dis.* 214, 707–711. <http://dx.doi.org/10.1093/infdis/jiw226>.

Ferron, F., Bussetta, C., Dutartre, H., Canard, B., 2005. The modeled structure of the RNA dependent RNA polymerase of GBV-C virus suggests a role for motif E in Flaviviridae RNA polymerases. *BMC Bioinforma.* 6, 255. <http://dx.doi.org/10.1186/1471-2105-6-255>.

Fung, A., Jin, Z., Dyatkina, N., Wang, G., Beigelman, L., Deval, J., 2014. Efficiency of incorporation and chain termination determines the inhibition potency of 2'-modified nucleotide analogs against hepatitis C virus polymerase. *Antimicrob. Agents Chemother.* 58, 3636–3645. <http://dx.doi.org/10.1128/AAC.02666-14>.

Gebhard, L.G., Filomatori, C.V., Gamarnik, A.V., 2011. Functional RNA elements in the dengue virus genome. *Viruses* 3, 1739–1756. <http://dx.doi.org/10.3390/v3091739>.

Gong, P., Peersen, O.B., 2010. Structural basis for active site closure by the poliovirus RNA-dependent RNA polymerase. *Proc. Natl. Acad. Sci. U. S. A.* 107, 22505–22510. <http://dx.doi.org/10.1073/pnas.1007626107>.

Gubler, D.J., 2011. Dengue, urbanization and globalization: the unholy trinity of the 21(st) century. *Trop. Med. Health* 39, 3–11. <http://dx.doi.org/10.2149/tmh.2011-S05>.

Gubler, D., Kuno, G., Markoff, L., 2007. *Flaviviruses*. In: *Fields Virology, fifth ed.* Lippincott-Raven Publishers, Philadelphia, USA, pp. 1155–1227.

Guy, B., Lang, J., Saville, M., Jackson, N., 2016. Vaccination against dengue: challenges and current developments. *Ann. Rev. Med.* 67, 387–404. <http://dx.doi.org/10.1146/annurev-med-091014-090848>.

Huang, Y., Beaudry, A., McSwiggen, J., Sousa, R., 1997. Determinants of ribose specificity in RNA polymerization: effects of Mn²⁺ and deoxynucleoside monophosphate incorporation into transcripts. *Biochem. Mosc.* 36, 13718–13728. <http://dx.doi.org/10.1021/bi971609o>.

Jin, Z., Deval, J., Johnson, K.A., Swinney, D.C., 2011. Characterization of the elongation complex of dengue virus RNA polymerase: assembly, kinetics of nucleotide incorporation, and fidelity. *J. Biol. Chem.* 286, 2067–2077. <http://dx.doi.org/10.1074/jbc.M110.162685>.

Jin, Z., Leveque, V., Ma, H., Johnson, K.A., Klumpp, K., 2012. Assembly, purification, and pre-steady-state kinetic analysis of active RNA-dependent RNA polymerase elongation complex. *J. Biol. Chem.* 287, 10674–10683. <http://dx.doi.org/10.1074/jbc.M111.325530>.

Kelley, L.A., Mezulis, S., Yates, C.M., Wass, M.N., Sternberg, M.J.E., 2015. The Phyre2 web portal for protein modeling, prediction and analysis. *Nat. Protoc.* 10,

- 845–858. <http://dx.doi.org/10.1038/nprot.2015.053>.
- Kibbe, W.A., 2007. OligoCalc: an online oligonucleotide properties calculator. *Nucleic Acids Res.* 35, W43–W46. <http://dx.doi.org/10.1093/nar/gkm234>.
- Klema, V.J., Ye, M., Hindupur, A., Teramoto, T., Gottipati, K., Padmanabhan, R., Choi, K.H., 2016. Dengue virus nonstructural protein 5 (NS5) assembles into a dimer with a unique methyltransferase and polymerase interface. *PLoS Pathog.* 12, e1005451. <http://dx.doi.org/10.1371/journal.ppat.1005451>.
- Latour, D.R., Jekle, A., Javanbakht, H., Henningsen, R., Gee, P., Lee, L., Tran, P., Ren, S., Kutach, A.K., Harris, S.F., Wang, S.M., Lok, S.J., Shaw, D., Li, J., Heilek, G., Klumpp, K., Swinney, D.C., Deval, J., 2010. Biochemical characterization of the inhibition of the dengue virus RNA polymerase by beta-d-2'-ethynyl-7-deazaadenosine triphosphate. *Antivir. Res.* 87, 213–222. <http://dx.doi.org/10.1016/j.antiviral.2010.05.003>.
- Lessler, J., Chaisson, L.H., Kucirka, L.M., Bi, Q., Grantz, K., Salje, H., Carcelen, A.C., Ott, C.T., Sheffield, J.S., Ferguson, N.M., Cummings, D.A.T., Metcalf, C.J.E., Rodriguez-Barraquer, I., 2016. Assessing the global threat from Zika virus. *Science*. <http://dx.doi.org/10.1126/science.aaf8160>.
- Lim, S.P., Koh, J.H.K., Seh, C.C., Liew, C.W., Davidson, A.D., Chua, L.S., Chandrasekaran, R., Cornvik, T.C., Shi, P.-Y., Lescar, J., 2013. A crystal structure of the dengue virus non-structural protein 5 (NS5) polymerase delineates inter-domain amino acid residues that enhance its thermostability and de novo initiation activities. *J. Biol. Chem.* 288, 31105–31114. <http://dx.doi.org/10.1074/jbc.M113.508606>.
- Lindenbach, B., Rice, C., 2007. *Flaviviridae: the viruses and their replication*. In: *Fields Virology*. Lippincott-Raven Publishers, pp. 1101–1151.
- Lindorff-Larsen, K., Piana, S., Palmo, K., Maragakis, P., Klepeis, J.L., Dror, R.O., Shaw, D.E., 2010. Improved side-chain torsion potentials for the Amber ff99SB protein force field. *Proteins* 78, 1950–1958. <http://dx.doi.org/10.1002/prot.22711>.
- Lu, G., Gong, P., 2013. Crystal Structure of the full-length Japanese encephalitis virus NS5 reveals a conserved methyltransferase-polymerase interface. *PLoS Pathog.* 9, e1003549. <http://dx.doi.org/10.1371/journal.ppat.1003549>.
- Pettersen, E.F., Goddard, T.D., Huang, C.C., Couch, G.S., Greenblatt, D.M., Meng, E.C., Ferrin, T.E., 2004. UCSF Chimera—a visualization system for exploratory research and analysis. *J. Comput. Chem.* 25, 1605–1612. <http://dx.doi.org/10.1002/jcc.20084>.
- Poranen, M.M., Salgado, P.S., Koivunen, M.R.L., Wright, S., Bamford, D.H., Stuart, D.I., Grimes, J.M., 2008. Structural explanation for the role of Mn²⁺ in the activity of phi6 RNA-dependent RNA polymerase. *Nucleic Acids Res.* 36, 6633–6644. <http://dx.doi.org/10.1093/nar/gkn632>.
- Potisopon, S., Priet, S., Collet, A., Decroly, E., Canard, B., Selisko, B., 2014. The methyltransferase domain of dengue virus protein NS5 ensures efficient RNA synthesis initiation and elongation by the polymerase domain. *Nucleic Acids Res.* 42, 11642–11656. <http://dx.doi.org/10.1093/nar/gku666>.
- Rasmussen, S.A., Jamieson, D.J., Honein, M.A., Petersen, L.R., 2016. Zika virus and birth defects—reviewing the evidence for causality. *N. Engl. J. Med.* 374, 1981–1987. <http://dx.doi.org/10.1056/NEJMs1604338>.
- Sali, A., Blundell, T.L., 1993. Comparative protein modelling by satisfaction of spatial restraints. *J. Mol. Biol.* 234, 779–815. <http://dx.doi.org/10.1006/jmbi.1993.1626>.
- Saw, W.G., Tria, G., Grüber, A., Subramanian Manimekalai, M.S., Zhao, Y., Chandramohan, A., Srinivasan Anand, G., Matsui, T., Weiss, T.M., Vasudevan, S.G., Grüber, G., 2015. Structural insight and flexible features of NS5 proteins from all four serotypes of Dengue virus in solution. *Acta Crystallogr. D. Biol. Crystallogr.* 71, 2309–2327. <http://dx.doi.org/10.1107/S1399004715017721>.
- Selisko, B., Dutartre, H., Guillemot, J.-C., Debarnot, C., Benaroch, D., Khromykh, A., Després, P., Egloff, M.-P., Canard, B., 2006. Comparative mechanistic studies of *de novo* RNA synthesis by flavivirus RNA-dependent RNA polymerases. *Virology* 351, 145–158. <http://dx.doi.org/10.1016/j.virol.2006.03.026>.
- Selisko, B., Potisopon, S., Agred, R., Priet, S., Varlet, I., Thillier, Y., Sallamand, C., Debart, F., Vasseur, J.-J., Canard, B., 2012. Molecular basis for nucleotide conservation at the ends of the dengue virus genome. *PLoS Pathog.* 8, e1002912. <http://dx.doi.org/10.1371/journal.ppat.1002912>.
- Shim, J.H., Larson, G., Wu, J.Z., Hong, Z., 2002. Selection of 3'-template bases and initiating nucleotides by hepatitis C virus NS5B RNA-dependent RNA polymerase. *J. Virol.* 76, 7030–7039.
- Tan, B.H., Fu, J., Sugrue, R.J., Yap, E.H., Chan, Y.C., Tan, Y.H., 1996. Recombinant dengue type 1 virus NS5 protein expressed in *Escherichia coli* exhibits RNA-dependent RNA polymerase activity. *Virology* 216, 317–325. <http://dx.doi.org/10.1006/viro.1996.0067>.
- Vashishtha, A.K., Wang, J., Konigsberg, W.H., 2016. Different divalent cations alter the kinetics and fidelity of DNA polymerases. *J. Biol. Chem.* 291, 20869–20875. <http://dx.doi.org/10.1074/jbc.R116.742494>.
- Wright, S., Poranen, M.M., Bamford, D.H., Stuart, D.I., Grimes, J.M., 2012. Non-catalytic ions direct the RNA-dependent RNA polymerase of bacterial double-stranded RNA virus phi6 from *de novo* initiation to elongation. *J. Virol.* 86, 2837–2849. <http://dx.doi.org/10.1128/JVI.05168-11>.
- Wu, J., Lu, G., Zhang, B., Gong, P., 2015. Perturbation in the conserved methyltransferase-polymerase interface of flavivirus NS5 differentially affects polymerase initiation and elongation. *J. Virol.* 89, 249–261. <http://dx.doi.org/10.1128/JVI.02085-14>.
- Zhao, Y., Soh, T.S., Chan, K.W.K., Fung, S.S.Y., Swaminathan, K., Lim, S.P., Shi, P.-Y., Huber, T., Lescar, J., Luo, D., Vasudevan, S.G., 2015a. Flexibility of NS5 methyltransferase-polymerase linker region is essential for dengue virus replication. *J. Virol.* 89, 10717–10721. <http://dx.doi.org/10.1128/JVI.01239-15>.
- Zhao, Y., Soh, T.S., Zheng, J., Chan, K.W.K., Phoo, W.W., Lee, C.C., Tay, M.Y.F., Swaminathan, K., Cornvik, T.C., Lim, S.P., Shi, P.-Y., Lescar, J., Vasudevan, S.G., Luo, D., 2015b. A crystal structure of the Dengue virus NS5 protein reveals a novel inter-domain interface essential for protein flexibility and virus replication. *PLoS Pathog.* 11, e1004682. <http://dx.doi.org/10.1371/journal.ppat.1004682>.
- Zmurko, J., Marques, R.E., Schols, D., Verbeken, E., Kaptein, S.J.F., Neyts, J., 2016. The viral polymerase inhibitor 7-deaza-2'-C-methyladenosine is a potent inhibitor of in vitro Zika virus replication and delays disease progression in a robust mouse infection model. *PLoS Negl. Trop. Dis.* 10, e0004695. <http://dx.doi.org/10.1371/journal.pntd.0004695>.
- Zuker, M., 2003. Mfold web server for nucleic acid folding and hybridization prediction. *Nucleic Acids Res.* 31, 3406–3415.